# CONFERENCE PRE-PRINT

# EXPERIMENTAL INVESTIGATION OF DEUTERIUM AND NITROGEN-SEEDED H-MODE PLASMAS IN KSTAR WITH A TUNGSTEN DIVERTOR AND CARBON FIRST WALL

J.H. HWANG, Y.S. HAN, S. BONG, C. SHIN, J.H. YOON, C. LEE, W. CHOE Korea Advanced Institute of Science and Technology Daejeon, Republic of Korea Email: wchoe@kaist.ac.kr

H.H. LEE, E.N. BANG, G.W. SHIN, J. JANG, H.-S. KIM Korea Institute of Fusion Energy Daejeon, Republic of Korea

R.A. PITTS, A. PSHENOV ITER Organization St Paul Lez Durance Cedex, France

M. KIM Princeton University Princeton, U.S.A.

J.-S. PARK Oak Ridge National Laboratory Oak Ridge, U.S.A.

Abstract

The paper reports on KSTAR experiments designed to study H-mode detachment and tungsten (W) transport with both deuterium (D) fuelling and nitrogen (N) seeding. The two gases produced distinct core and edge responses. With D fuelling alone, strong detachment is not achieved in these ELMing H-mode plasmas with 6 MW of additional heating power, but there is a clear transition to near complete detachment with strong enough N seeding, manifest by an abrupt collapse of the outer target plate electron temperature. The behaviour of plasma radiation also differed with injected species, especially in the confined plasma. Deuterium fuelling led to only modest increases in core radiation, whereas N<sub>2</sub> seeding produced substantial core radiation with pronounced on-axis peaking of W density. This is consistent with the collisionality dependence of neoclassical temperature screening (weakened at higher collisionality). Overall, in the discharges studied, N is effective at promoting divertor detachment, but tends to exacerbate core W accumulation, implying that additional control of inward W transport is needed to achieve core-edge compatible detached operation with N<sub>2</sub> seeding in KSTAR with the W divertor.

# 1. INTRODUCTION

The new, actively cooled, W divertor in KSTAR aims to permit long pulse, high power operation using ITER-relevant monoblock technology but maintaining as much as possible the ability to operate with the same or similar plasma configurations developed during the years with the previous carbon (C) divertor [1]. It differs slightly with respect to the previous C variant in that inner neutral baffling is somewhat improved and operation with vertical inner and outer divertor target geometry is now favoured (though it is still possible to run with inner vertical, outer "central divertor" configurations). Given the switch of materials and the change of divertor geometry, it is important to characterise the divertor plasma, particularly with regard to detachment and here we report some results from the first experiments executed to investigate the D-fuelled and N-seeded H-mode discharges which have been found to provide the best performance in previous studies with the C divertor [2]. During the gas injection, changes in W impurity behaviour have been observed. These will be analysed in the context of neoclassical transport. An important caveat is to note that for these experiments KSTAR is still operating with C first wall armour, so the plasma-facing components are a mix of C and W, similar to the situation explored for a short time in ASDEX Upgrade in the late 1990's [3].

# 2. EXPERIMENTAL DISCHARGES

Target deuterium H-mode discharges were operated with 6.0 MW of total heating power (5.0 MW neutral beam injection (NBI) and 1.0 MW on-axis electron cyclotron heating (ECH)) at plasma current of  $I_p = 0.5$  MA and toroidal magnetic field of  $B_t = 1.9$  T, giving  $q_{95} \sim 5.8$ . The magnetic configuration (Fig. 1(a)) was lower single-null, with the outer strike point on the outer vertical divertor and the ion  $B \times \nabla B$  drift toward the active lower X-point. Gas injection rates ( $\Gamma_{D2}$  and  $\Gamma_{N2}$ ) were varied between the discharges, in the range of  $\Gamma_{D2} = 2.2 \times 10^{20} - 5.0 \times 10^{20}$  atoms/s and  $\Gamma_{N2} = 1.0 \times 10^{20} - 1.7 \times 10^{20}$  atoms/s. For each discharge, a constant rate was applied from 8.0 s to 14.0 s, with the latter being time at the end of the current flat-top. All shots followed a W-avoidance scenario [4], in which divertor D-fuelling, shaped heating waveforms, and early-phase (< 7.0 s) plasma shape control were incorporated, to limit core W accumulation and resulting H-L dithering. Three representative cases were selected: a reference (Shot #35490,  $\Gamma_{D2} = 2.2 \times 10^{20}$  atoms/s), a more strongly D-fuelled case (Shot #35491,  $\Gamma_{D2} = 3.8 \times 10^{20}$  atoms/s), and an N-seeded case (Shot #35499,  $\Gamma_{N2} = 1.7 \times 10^{20}$  atoms/s) without D-fuelling. These had comparable upstream profiles prior to 8.0 s, when no seeding was applied. In the reference shot (with the lowest D-fuelling), the key plasma parameters shown in Fig. 1b hardly changed so it is treated as the non-seeding condition. Fig. 1(a) gives an example magnetic equilibrium of the reference discharge (#35490) at 7.5 s overlaid with the key diagnostics used in the study.

Fig. 1(b) summarizes the time traces for the three discharges. With increased D-fuelling (blue, referred henceforth as D<sub>2</sub>), the upstream line-averaged density ( $\bar{n}_e$ ) and total radiated power ( $P_{rad,tot}$ ) remain essentially unchanged through to the end of the discharge, with the confinement ( $H_{98(y,2)}$ ) falling by ~20% relative to the non-injection phase (7.0-8.0 s). With N-seeding (red, referred to as N<sub>2</sub>),  $\bar{n}_e$  is again roughly constant through the flattop, but  $P_{rad,tot}$  increases to ~50% of  $P_{heat}$  and  $H_{98(y,2)}$  decreases strongly by ~50%. In both the D-fuelled and N-seeded cases, WI emission along a line-of-sight through the inner divertor weakens after gas injection, with a larger reduction for N injection. For the higher D-fuelled discharge, the ELM frequency  $f_{ELM}$  increased by up to a factor of ~2 from an initial ~90 Hz, accompanied by smaller ELMs, probably indicating a Type I – Type III transition (Fig. 1(c)). In contrast, the N-seeded discharge, there is a clear, abrupt transition to higher frequency ELMs (likely Type III) at ~9.3 s, with  $f_{ELM}$  thereafter between 100-500 Hz. Although N seeding has improved core performance in full-W tokamaks by behaving similarly to the situation in a full-C device where C provides the radiating impurity [5,6], this trend is not observed in KSTAR with a W divertor, indicating that the remaining C walls (limiters and upper divertor) still play a substantial role.

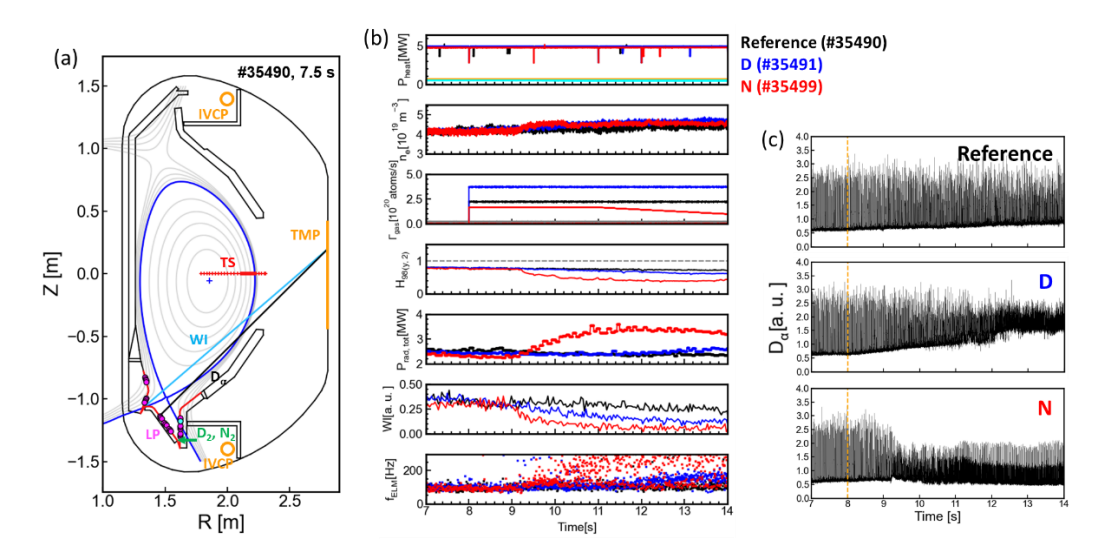


Fig. 1 (a) Magnetic equilibrium of the reference discharge (Shot #35490, 7.5 s) with diagnostics used in the study labelled: the Thomson scattering system (TS) and the tile-embedded Langmuir probes (LP), along with lines-of-sight of the visible spectrometer for WI line emission measurement (WI) and the poloidal  $D_{\alpha}$  monitoring system ( $D_{\alpha}$ ). The locations of  $D_{2}$  and  $N_{2}$  gas puffs are also shown. Orange lines depict the locations of the top and bottom in-vessel cryo-pumps (IVCPs), and the pumping duct connected to the turbo-molecular pump (TMP). The red line represents the contour of the W monoblock divertor target. (b) Time evolution of experimental plasma parameters for the reference (Shot #35490, black), D-fuelled (Shot #35491, blue) and N-seeded (Shot #35499, red) discharges: total heating power  $P_{heat}$  (cyan and orange lines give  $P_{ECH}$  with the majority of  $P_{heat}$  is due to NBI), line-averaged electron density ( $\bar{n}_{e}$ ), gas injection rates ( $\Gamma_{gas}$ ), H-factor ( $H_{98(y,2)}$ ), total radiated power ( $P_{rad,tot}$ ), inter-ELM WI line emission intensity (WI), and ELM frequency ( $f_{ELM}$ ). (c)  $D_{\alpha}$  line emission intensity for the three discharges showing the change in ELM behaviour as gas is injected.

# 3. DETACHMENT EVOLUTION AND RADIATION DISTRIBUTION

Figure 2 compiles some experimental Langmuir probe signals for the three discharges in Fig. 1. For a probe at or near the outer strike point (see Fig. 2(c)), there is clearly no significant change in the target ion flux (j<sub>sat.out</sub>) baseline for the two D-fuelled cases, indicating that in these particular H-modes with  $P_{heat} = 6$  MW, detachment cannot be achieved with fuelling alone. In the case of strong N-seeding, the strong transition seen in the  $D_{\alpha}$  signal (Fig. 1(c)) is as expected also observed in the  $j_{sat,out}$  trace, indicating strong strike point detachment. This is also reflected in the electron temperature  $(T_{et})$  behaviour seen on a Langmuir probe ~4 cm from the outer strike point along the target, which is the only voltage scanned probe available in these discharges from which a plasma temperature can be extracted (Fig. 2(b)). Whilst there is no change at this mid-scrape-off layer (SOL) Tet. for the reference case, with higher D-fuelling, the temperature does eventually fall to low values and collapses abruptly in the N-seeded case only ~1 s after the impurity injection begins. This, together with the coincident strong reduction in strike point ion flux is indicative of complete detachment across the target when at these levels of impurity injection, also consistent with the change in ELM character and the strong reduction in confinement. The outer target ion flux profiles in Fig. 2(d) also indicate the reduction in strike point ion flux, but do not show strong ion flux detachment deeper in the divertor SOL. These profiles are obtained by small outer strike point sweeps across the available probes, but this sweeping was not applied in the high N-seeding case discussed here (pulse #35499). The profile during N-seeding shown in Fig. 2(d) was instead obtained in a discharge with lower N<sub>2</sub> injection and this may explain the higher main SOL ion flux. It is also the case that ELM filtering is applied to produce these profiles and when  $f_{ELM}$  increases strongly, there are no longer clear inter-ELM phases and the ion current baseline increases.

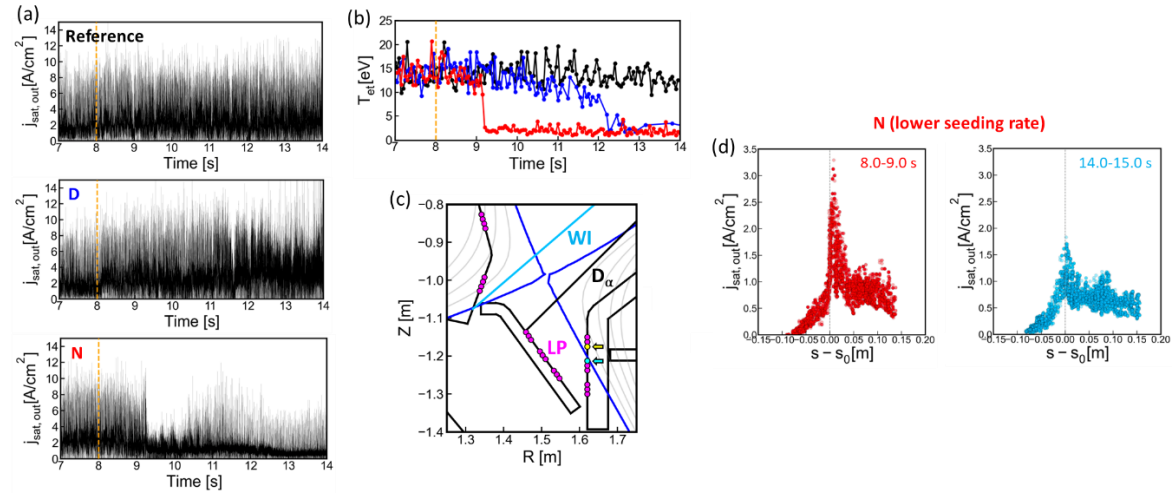


Fig. 2 (a) Outer target ion saturation current density ( $j_{sat,out}$ ) measured by a Langmuir probe with fixed negative bias voltage at the separatrix and (b) electron temperature ( $T_{et}$ ) measured by a voltage sweeping probe ~4 cm outside the separatrix for the reference, D-fuelled, and N-seeded discharges. The orange dashed lines represent the onset of gas injection. (c) Poloidal locations of the tile-embedded array of Langmuir probes. The probes with fixed and sweeping voltage used in (a) and (b) are depicted as cyan and yellow colours, respectively. (d) Radial profiles of  $j_{sat,out}$  for the N-seeding case with lower seeding rate (note that for these profiles, ELM filtering has been applied in contrast to the raw data shown in (a)).

The two-dimensional distributions of total radiated power  $P_{rad,tot}$  for the three pulses are compared in Fig. 3. In the divertor, the reference case shows a strong peak at the inner target with no significant emission at the outer divertor. With increased D-fuelling, the radiation front appears to move toward the X-point, indicating plasma cooling in front of the inner target. During N-seeding, the front extends horizontally into the outer SOL and above the X-point. In the core, there are very weak indications for enhanced radiation on the low-field-side (LFS), possibly increasing slightly at higher D-fuelling. In contrast,  $N_2$  seeding leads to a very significant increase in core radiation with pronounced on-axis peaking.

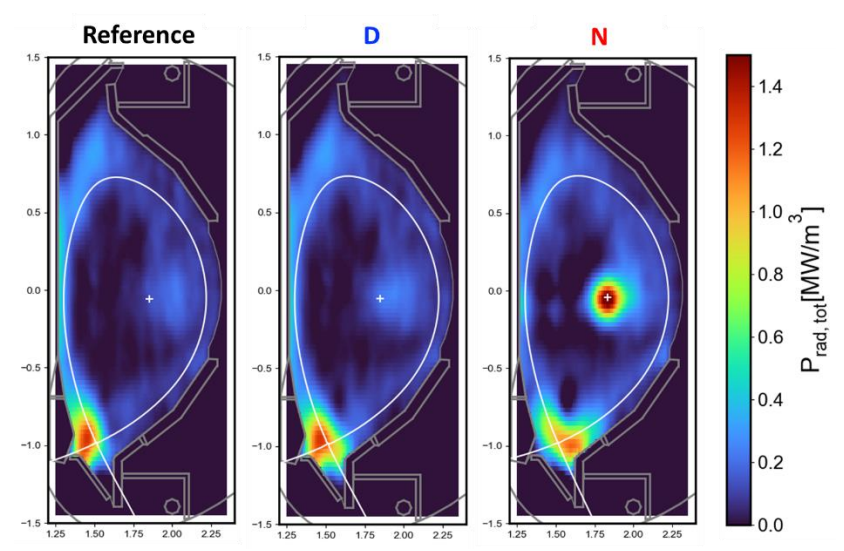


Fig. 3 Two-dimensional distributions of  $P_{rad,tot}$  averaged over 12.9-13.4 s for the three selected discharge.

# 4. CORE TUNGSTEN IMPURITY BEHAVIOR

The core tungsten density  $n_W$  was estimated to examine impurity transport using the relation,  $n_W = P_{rad,tot}/n_e L_W$ , where  $n_e$  is the electron density and  $L_W$  is the W cooling factor (radiation efficiency) [7], dependent on  $T_e$ . Figure 4(a)-(b) present radial  $n_W$  profiles before and after gas injection. The analysis assumes core radiation is exclusively from W, which can be misleading for r/a > 0.8 due to the strong X-point radiation, especially in the  $N_2$  case. Thus, the profiles are shown only up to r/a = 0.8. Differences in the  $n_W$  profiles among the three discharges are consistent with those observed in the radiation patterns. With higher D-fuelling,  $n_W$  increases slightly near the magnetic axis compared to the reference case, whereas N-seeding produces a much larger increase, reaching up to  $n_W \sim 10^{-2} \times \bar{n}_e$ . This increase extends across a wide portion of the plasma radius and is most pronounced near the magnetic axis. The on-axis peaking increases with time during the N-seeding (Fig. 4(c)). The much higher W concentrations and on-axis peaking seen in the impurity seeded discharge clearly indicates a change in W transport with enhanced inward convection. It is worthwhile noting that, as shown in Fig. 4(a) and (b), in the reference and higher D-fuelled cases  $n_W$  was lower in the later time window (12.9-13.4 s) than earlier (7.0-7.5 s), possibly due to ELM flushing [8].

As reported in [9], neoclassical temperature screening weakens and can even reverse (leading to temperature peaking), as background ion collisionality increases. Since the ion-ion collision frequency scales as  $v_{ab} \propto Z_a^2 Z_b^2$ , N-W collisions dominate D-W collisions, so background N largely governs neoclassical W transport. Under continuous N-seeding, collisionality increases due to the higher N content. A consequent rise in core W content lowers core  $T_i$  which further increases collisionality, creating a positive feedback cycle which reduces temperature screening. Modelling with the NEO [10,11] code is planned to validate and refine these interpretations.

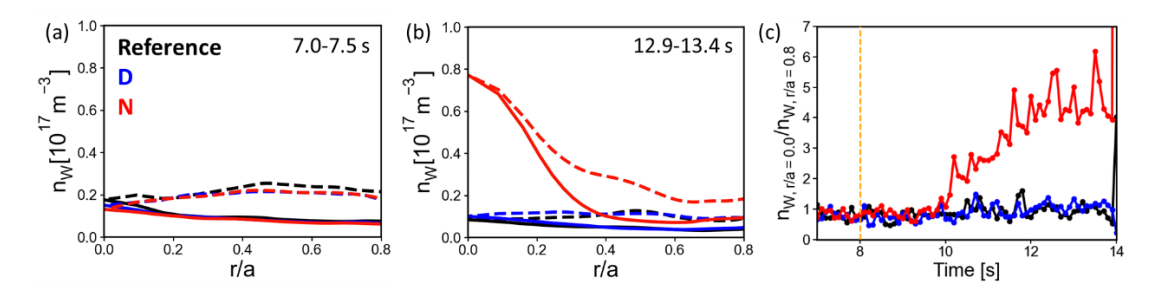


Fig. 4. W density  $(n_W)$  profiles averaged over (a) 7.0-7.5 s (before gas injection) and (b) 12.9-13.4 s (after gas injection). The solid lines show flux surface averaged profiles, while the dashed lines show LFS profiles. (c) Time evolution in the 3 pulses of the on-axis peaking of  $n_W$  calculated as  $n_{W,r/a=0.0}/n_{W,r/a=0.8}$ .

# 5. CONCLUSIONS

Gas injection experiments in Type I ELMing H-modes with the new lower W divertor in KSTAR (but still with carbon first wall plasma-facing components) show distinct core and edge plasma responses to D-fuelling and N-seeding. Even strong D-fuelling is unable to produce much, if any detachment at the outer divertor targets for the 6 MW input power discharges studied. In contrast, with N-seeding, abrupt ("cliff edge") decreases in both target ion flux and plasma electron temperature are observed beyond a given seeding level, indicating strong detachment, probably due to power exhaustion as a consequence of strong radiation in the X-point vicinity. Unsurprisingly, this divertor collapse and X-point radiation is associated with a significant reduction in confinement and a transition to rapid, smaller ELMs, indicating proximity to an H-L back transition. Core radiation is also significantly impacted by N-seeding, which provokes strong on-axis peaking attributed to increased W concentrations. This behaviour is consistent with weakened neoclassical temperature screening at higher ion-ion collisionality induced by the N impurity. Additional heating by neutral beam injection and/or ion cyclotron resonance heating could mitigate the issue by increasing  $T_i$ , thereby lowering collisionality and strengthening temperature screening. Modelling with SOLPS-ITER [12] and NEO codes is planned to validate and refine these interpretations of divertor and core response.

# **ACKNOWLEDGEMENTS**

This work was supported by the National Research Foundation of Korea (NRF) funded by the Korean government (Ministry of Science and ICT) (RS-2022-00155960) and R&D Program of "Development of SOL-divertor operation scenarios in burning plasma regime for conceptual design of fusion reactor (CN2502-2)" through the Korea Institute of Fusion Energy (KFE) funded by the Government funds. The views and opinions expressed herein do not necessarily reflect those of the ITER Organization. The author wishes to thank Choongseok Chang for valuable comments on neoclassical W transport.

# REFERENCES

- [1] LEE, H.H., et al., "Study on the tungsten source and transport during the first operation of the tungsten cassette monoblock divertor in the KSTAR tokamak", 3<sup>rd</sup> International Fusion and Plasma Conference, Seoul (2024).
- [2] HWANG, J.H., et al., "Low Z impurity seeding in KSTAR H-mode plasmas", 64<sup>th</sup> Annual Meeting of the APS Division of Plasma Physics, Spokane, Washington (2022).
- [3] NEU, R., et al., The tungsten experiment in ASDEX Upgrade, J. Nucl. Mater. 241-243 (1997) 678.
- [4] KIM., S.K., et al., "Summary on developing W-avoidance strategy", 2024 KSTAR Campaign Summary Meeting, Daejeon, 2025.
- [5] BEURSKENS, M.N.A., et al., The role of carbon and nitrogen on the H-mode confinement in ASDEX Upgrade with a metal wall, Nucl. Fusion 56 (2016) 056014.
- [6] DUNNE, M.G., Impact of impurity seeding and divertor conditions on transitions, pedestal structure and ELMs, Nucl. Fusion 57 (2017) 025002.
- [7] PÜTTERICH, T., et al., Calculation and experimental test of the cooling factor of tungsten, Nucl. Fusion 50 (2010) 025012.
- [8] PÜTTERICH, T., et al., ELM flushing and impurity transport in the H-mode edge barrier in ASDEX Upgrade, J. Nucl. Mater 415 (2011) S334-S339.
- [9] FAJARDO, D., et al., Analytic model for the combined effects of rotation and collisionality on neoclassical impurity transport, Plasma Phys. Control. Fusion 65 (2023) 035021.
- [10] BELLI, E.A. and CANDY, J., Kinetic calculation of neoclassical transport including self-consistent electron and impurity dynamics, Plasma Phys. Control. Fusion 50 (2008) 095010.
- [11] BELLI, E.A. and CANDY, J., Full linearized Fokker-Planck collisions in neoclassical transport simulations, Plasma Phys. Control. Fusion 54 (2012) 015015.
- [12] WIESEN, S., et al., The new SOLPS-ITER code package, J. Nucl. Mater. 463 (2015) 480-484.